 doi:10.20944/preprints202102.0288.v1

*Article*

# Coordinated Adaptive Directional Overcurrent Protection System for AC Microgrids

**Noor Hussain [1,2], Mashood Nasir [1], Yousef Khayat [1], Juan Carlos Vasquez [1] and Josep M. Guerrero [1,*]**

[1] Center for Research on Microgrids (CROM), Department of Energy Technology, Aalborg University 9220 Aalborg, Denmark; nhu@et.aau.dk (N.H.); mnas@et.aau.dk (M.N.); ykh@et.aau.dk (Y.K), juq@et.aau.dk (J.C.V.); joz@et.aau.dk (J.M.G.)

[2] Engineering Department, Balochistan University of Engineering and Technology Khuzdar 89100, Pakistan.

* Correspondence: * joz@et.aau.dk; Tel.: (+45)-2037-8262

**Abstract:** In this research work, an adaptive scheme for the coordinated protection of AC Microgrids using directional overcurrent (DOCR) relays is presented. Protection of AC MGs is a complex and challenging issue due to the dynamic nature of the network including, a) its capability to reconfigure the modes of operation ranging from grid-connected to the islanded mode, c) bidirectional-power flow capability, and c) integration of intermittent renewable energy resources with real-time variations in the resource availability. Consequently, the fault current contributions may largely vary depending upon the incident conditions on the network. Conventional protection schemes, generally designed for radial networks, and unidirectional power flow from the source end to the load may either mal-operate or exhibit very poor performance, if not adapted according to the dynamic conditions of the network. To address this issue, a communication-based adaptive protection scheme capable to adapt its settings according to the generation resource availability and network configuration is presented in this work. The proposed scheme consists of an intelligent central protection unit (ICPU) capable to update the settings and communicate it to the individual relays based on the pre-calculated offline settings. The directional overcurrent relays employed in the scheme use two-stage settings, i.e. definite time and inverse definite minimum time characteristics for the effective coordination among the downstream and upstream relays. An adaptive algorithm for ICPU operation is presented and a case study is implemented for a modified IEEE 9-bus system using DigSilent Power factory. The results for various scenarios including, a) grid-connected mode of operation, b) islanded mode of operation, and c) variable distributed generation mode are obtained and compared to the static scheme, which validates the effectiveness of the proposed scheme.

**Keywords:** Adaptive Protection; Fault Detection; Microgrids; Directional Overcurrent Relay

## 1. Introduction

Due to worldwide growing demands of sustainable, environmentally friendly, and green energy, renewable energy resources (RESs) such as wind turbines (WT) and Photovoltaic (PV) are being deployed extensively [1, 2]. According to the international energy agency (IEA), generation from renewable energy resources will surpass the generation from coal by 2025 [3]. The integration and utilization of RESs in the conventional distribution system network developed the concept of Microgrids (MGs). MGs are emerging as an innovative approach to integrate as well as coordinate the energy supply from RESs to the utility grid such as grid-connected and operate in islanded mode.

MGs provide countless benefits such as generation and utilization of energy near to consumer premises (long transmission and distribution line cost can be avoided ), which improves the power quality (during a weak grid condition), continues the energy supply (if the grid is disconnected),

enhance the energy efficiency, increases the system reliability, and balance energy supply/demand by energy sharing (Multiple MGs system) [4, 5]. Regardless of many countless benefits of MGs systems, there are still various operational and technical challenges that are needed to investigate such as control, monitoring, energy management, security from cyber-attacks, and protection [5].

The conventional power systems are generally radial in nature, and the flow of power is unidirectional, i.e. from the source end to the load end. Although differential and distance protection schemes are also commonly used in conventional power systems [6], however, directional overcurrent protection schemes are generally employed for the distribution feeder protection. Therefore, the focus of this work is mainly limited to directional overcurrent protection settings for the feeder and distribution line protection. These settings mainly include pick-up current, time multiplier setting (TMS), and coordination time interval (CTI). The conventional distribution network overcurrent protection schemes with static settings do not take into consideration the impact of varying network conditions, and therefore cannot be directly applied to MGs. On the other hand, protection of MGs is complex and challenging due to its dynamic nature including a) multi-mode operation e.g., grid-connected and islanded modes, b) bidirectional power flow capability, and c) changing short circuit power due to low and high inertia DGs that results in varying fault current contributions [7]. Furthermore, low level of fault current in islanded operation, high impedance faults (HIF), MGs network configuration changes such as connection and disconnection of DGs (plug and play characteristics) also result in varying fault contributions and short circuit capabilities [7]. Therefore, a protection scheme capable to adapt its settings based on the varying network conditions is highly desirable to ensure the safe and reliable operation of MGs [7].

Various researchers have worked on the adaptive protection settings for distribution networks integrated with high inertia-based distributed generation (DG) resources, e.g. synchronous generators. Mahat *et al.* [8] proposed a simple and adaptive protection to update the settings of overcurrent in distribution systems with DGs. As a case study, the authors have used a part of the distribution network by Himmerlands Elforsyning in Aalborg Denmark. The scheme uses local information of the variables and therefore avoids communication requirements; however, the configuration of the network is pre-known and does not change significantly due to the selected nature of the practical case studies. For distribution networks, having DGs dispersed at different locations generally requires global information of the network for accurate up-gradation of settings; therefore, having local information may not be sufficient and communication requirements may not be avoided for the universal application of this algorithm. Alternatively, Cofelle *et al.* [9] presented a communication-based online adaptive protection scheme for active management and islanded mode of operation for the distribution network. The scheme employs an inverse definite minimum time (IDMT) over current protection that may adopt its settings based on the mode of operation and compares its results with conventional overcurrent schemes. The proposed scheme largely relies on the real-time calculations for updating the settings of the relay. With the higher number of nodes and bigger size of the network, the proposed algorithm may take a long time to converge to the new settings, and therefore is not very suitable for larger networks. Alternatively, recently, Memon *et al.* [10] proposed an offline algorithm for adaptive protection of radial MGs using IEC 61850 communication standard, however, the proposed scheme is valid for radial MGs only, it does not cater to the protection needs for the emerging meshed MGs systems. Moreover, many researchers have also used artificial intelligence and machine learning techniques, e.g. artificial neural networks (ANN), and fuzzy logic (FL), and other optimization algorithms for the dynamic computation of overcurrent protection settings [11-14]. However, all these techniques are computationally extensive and require complicated infrastructural requirements for their real-world application. Based on the above-presented literature and highlighted limitations, it may be concluded that for effective overcurrent protection of AC MGs, we need a communication-based adaptive algorithm that can deal with multiple configurations, computationally less expensive, and is suitable for practical applications. In line with these requirements, we propose an adaptive directional overcurrent protection scheme in this work that uses offline computations to update the settings of individual relays. The careful selection of two-stage settings in directional overcurrent relays allows us to

Preprints (www.preprints.org) | NOT PEER-REVIEWED | Posted: 11 February 2021 doi:10.20944/preprints202102.0288.v1



achieve improved performance in terms of reduced tripping times. The scheme maintains its coordination for both islanded and grid-connected modes of operations, and valid for both radial and meshed/interconnected configurations. Moreover, the proposed scheme also tackles the variations in renewable distributed generation resource and is simple to implement for practical applications. The proposed methodology including the DOCR relay setting and adaptive protection algorithm is implemented by using the IEEE-9 bus system in DigSilent power factory. The simulation result shows that the method is reliable and can effectively detect fault conditions in a fast, selective, and coordinated manner.

The rest of the paper is organized as follows. Section 2 presents the proposed method for the dual setting of DOCR along with the implementation of the proposed adaptive protection scheme. Section 3 presented the simulation test model and specifications. Section 4 presents the test simulation results for various operation scenarios. The scheme also compares the results with the static settings to validate its effectiveness. Discussion of the results is also detailed in this section. Based on the results and discussions, the conclusion along with some future directions are detailed in Section 5.

## 2. Proposed Adaptive Protection Scheme Design

Figure 1. shows a generalized *N*+1 bus MGs model connected to the main grid through the point of common coupling (PCC) along with the proposed adaptive scheme for the overcurrent protection of the distribution lines. The MGs contains *N* number of DG units and loads connected to each bus as can be seen in figure 1. Moreover, the network is flexible and can be either connected in a radial or meshed configuration based on the position of the switch. For the protection of each line, there are two directional relays, where $R_f$ corresponds to the forward relay and $R_r$ corresponds to the reverse relay.

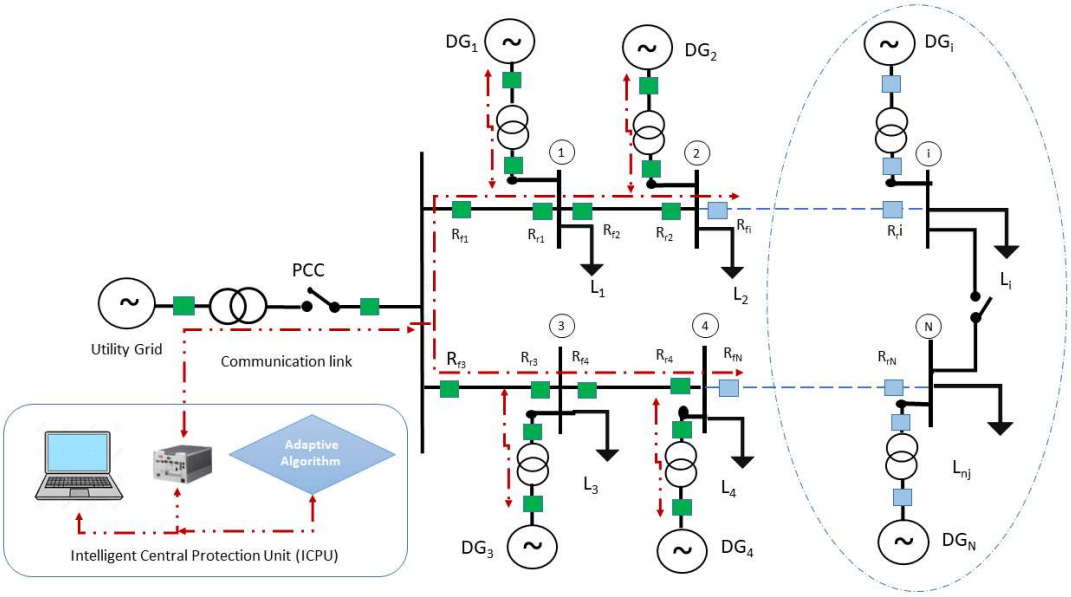


Figure 1: Adaptive Protection Scheme for generalized *N*-bus Microgrid.

The forward relays are sensitive to downstream faults and coordinates with other downstream forward relays only. Similarly, the reverse relays are sensitive to upstream faults and coordinates with other upstream relays only. The pick-up current settings, time multiplier settings (TMS), and coordination time interval (CTI) for the operation and coordination of each relay are determined according to the network configuration and operation scenarios as discussed in subsection 2.1. These sets of settings are computed and stored in the intelligent central protection unit (ICPU). Modern digital relays have the capability to store up to 8 group settings [15, 16], while ICPU containing the adaptive algorithm also keeps on monitoring the status of the network and updating the relay settings using the communication network (shown by the dotted lines). IEC 61850 standard is

Preprints (www.preprints.org) | NOT PEER-REVIEWED | Posted: 11 February 2021 doi:10.20944/preprints202102.0288.v1



generally employed for the communication among the protective devices [10]. The adaptive algorithm (presented in subsection 2.2) selects the right sets of setting according to the incident conditions on the network, and therefore, ICPU updates the relay settings accordingly.

### *2.1. Dual Stage Settings of DOCR*

As shown in figure 1 each line is protected by two relays, i.e. forward relay and reverse relay. For conventional power systems, generation is largely based on synchronous generators, therefore, short circuit capacity, fault current contributions from the synchronous generators and the associated relay settings (Pickup, TMS, and CTI) can be easily determined. The desired protection coordination can also be easily achieved using single-stage characteristics, i.e. either inverse characteristics or definite time characteristics. However, due to the dynamic characteristics of MGs, short circuit contribution is largely varying due to intermittent RESs and power electronics inverter interfacing. Moreover, mode of operation, i.e. grid-connected or islanded will also largely affect the short circuit contributions, for example, the short circuit current contribution in the grid-connected mode will be very high due to the large short circuit capacity of the grid, and is very small in the islanded mode due to limited short circuit capacity of the interfacing inverters. Also, the DG size, its location, fault type, and direction of the fault results in varying fault current contribution in the MGs. Therefore, single-stage settings are not feasible for microgrid operation. Alternatively in this scheme, we have employed dual-stage settings to deal with the varying short circuit contributions and also to maintain the desired coordination among upstream and downstream relays. The Figure 2. Shows the characteristics curve for the dual setting of DOCR, where stage 1 corresponds to the IEC 60255 standard inverse time relays characteristics [17] and is used for protection against short circuits and overloads, i.e. pickup time is inversely proportional to the fault current. The pick-up time of stage 1 is set according to (1) based on the line loading determined through the power flow analysis, while its time characteristics are set according to the ratio of fault current seen by the relay and maximum fault current as shown in (2).

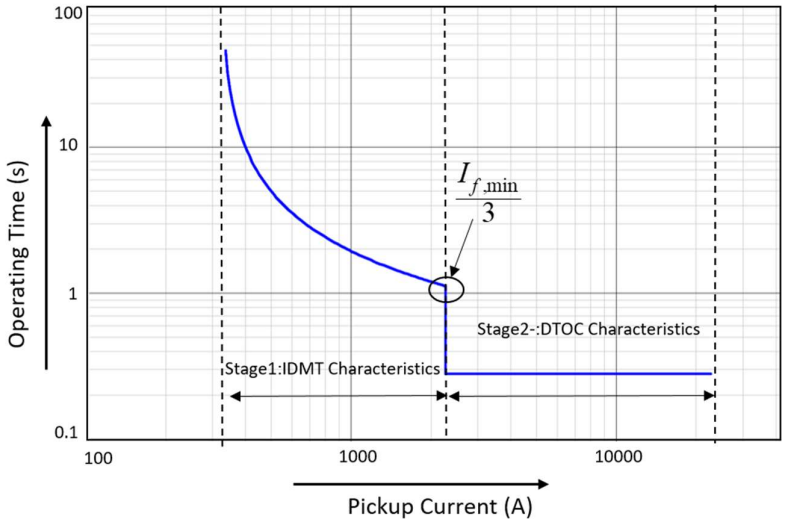


Figure 2: dual-stage settings of DOCR.

$$I^{1}_{pu,i} = (1 + k_1) \times I_{L,i} \quad (1)$$

Where, $i$ subscript corresponds to the $i^{th}$ relay in $N$ bus MGs model (refer to figure 1), and 1 superscript corresponds to stage 1. So, $I_{pu,i}{}^{1}$ is the pickup time of $i^{th}$ forward ($R_{if}$) or reverse ($R_{ir}$) relays for stage 1, $I_{L,i}$ is the loading of the line loading current of $i^{th}$ line, determined through power flow analysis, and $k_1$ is the allowable overloading threshold ranging from 0.5 to 1.

Preprints (www.preprints.org) | NOT PEER-REVIEWED | Posted: 11 February 2021 doi:10.20944/preprints202102.0288.v1



$$T_{op,i}^{1} = TMS_{i}^{1} \times \frac{A}{\left(\frac{I_{F,i}}{I_{pu,i}^{1}}\right)^{B} - 1} \quad (2)$$

Where $T_{op,i}^{1}$ is the trip time for $i^{th}$ forward ($R_{fi}$) or reverse ($R_{ri}$) relays for stage 1, $TMS_{i}^{1}$ is the time multiplier setting for $i^{th}$ Relay is stage 1, $I_{F,i}$ is the fault current seen by the $i^{th}$ relay, A and B are the constants based on which the slope of Inverness may be varied from standard inverse to extremely inverse characteristics. In the scope of this work, we have kept the characteristics to standard IEC inverse settings [17].

Similarly, stage 2 corresponds to the DTOC characteristics, its pickup time is determined using short circuit faults computed by short circuit analysis. Since fault current may vary based upon the type of fault, therefore we have adjusted the pickup settings for $i^{th}$ forward or reverse relay according to the minimum short circuit fault $I_{F\,min,i}$, which is also the boundary for two stages as shown in figure 2.

$$I_{pu,i}^{2} = \frac{I_{F\min,i}}{3} \quad (3)$$

The tripping logic for the dual-stage DOCR is shown in figure 3, where the combination of DTOC (IEEE/ANSI-50), and DOCR (IEEE ANSI-67) is coordinated through OR and AND gates.

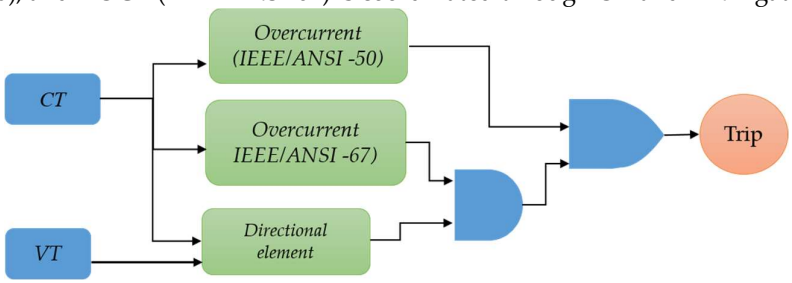


Figure 3: Trip logic for dual-stage DOCR.

The relay current transformer (CT) and voltage transformer (VT) measures current and voltages according to the predefined turn ratio settings, and the directional element decides the direction of the fault to be observed, either in the forward or in the reverse direction, based on whether its a forward relay or reverse relay in the network.

Lastly, the coordination settings of all the forward and reverse relays are determined using the coordination time interval between 0.3 and 0.4 seconds as specified by IEEE 242-2001 [18]. For stage 1 forward relays the relay at the farthest end is to be chosen as fastest, so according to IEC standard relay characteristics curves, TMS is selected as the lowest, i.e. 0.05, and operating time is determined using (2). The TMS for the consecutive upstream relays working in the forward direction is determined using (4).

$$TMS_{fi-1}^{1} = \frac{T_{fi}^{1} + CTI^{1}}{\left(\frac{I_{fi-1}}{I_{pu,i-1}^{1}}\right)^{B} - 1} \quad ;\forall i \in [2, N] \quad (4)$$

Similarly, for reverse relays, the nearest relay, is considered as the fastest with the lowest value of TMS, and the downstream reverse relays are designed using (5).

Preprints (www.preprints.org) | NOT PEER-REVIEWED | Posted: 11 February 2021 doi:10.20944/preprints202102.0288.v1



$$TMS^{1}_{ri+1} = \frac{T^{1}_{fi} + CTI^{1}}{\dfrac{A}{\left(\dfrac{I_{ri+1}}{I^{1}_{pu,i+1}}\right)^{B} - 1}} \quad ;\forall i \in [1, N-1] \tag{5}$$

For Stage 2, since we have definite time characteristics, therefore, CTI is maintained using a relatively lower value of CTI. Therefore, trip time for each consecutive forward upstream and each reverse downstream relay is given by (6):

$$T^{2}_{op,fi-1} = T^{2}_{op,fi} + CTI \quad ;\forall \mathrm{i} \in [2, N] \tag{6}$$

$$T^{2}_{op,ri+1} = T^{2}_{op,ri} + CTI \; ; \forall \mathrm{i} \in [1, N-1] \tag{7}$$

The trip time, TMS, and pickup times selected according to (1) - (7) ensure that proper coordination is maintained such that if one of the relays becomes faulty, or is unable to detect the fault, the consecutive relay waits for the defined time and then generates the backup tripping action as will be demonstrated in the result section.

### *2.2. Offline calculations and Adaptive Algorithm*

As discussed earlier, the main challenge with the microgrid overcurrent protection is due to its dynamic nature, its capability to operate in islanded as well as grid-connected mode, and the presence of DGs that may contribute to short circuit power in forward as well as reverse directions. Therefore, based on various possible configurations, and general operation scenarios, relay settings are calculated using (1) – (7) and following the flow chart shown in figure 4. The major steps involved in offline calculations are network identification, which corresponds to the state of the network, whether it is grid-connected, or islanded. The second step involves network parameter estimations including the capacity of DGs and their location in the network. It should be highlighted that the fault contribution from DGs is highly contingent on its location, particularly in the islanded mode. Therefore, the presence of DGs, their capacities, and location are determined in this step. Moreover, other network parameters including interconnection impedances are also determined in this step.

Preprints (www.preprints.org) | NOT PEER-REVIEWED | Posted: 11 February 2021 doi:10.20944/preprints202102.0288.v1



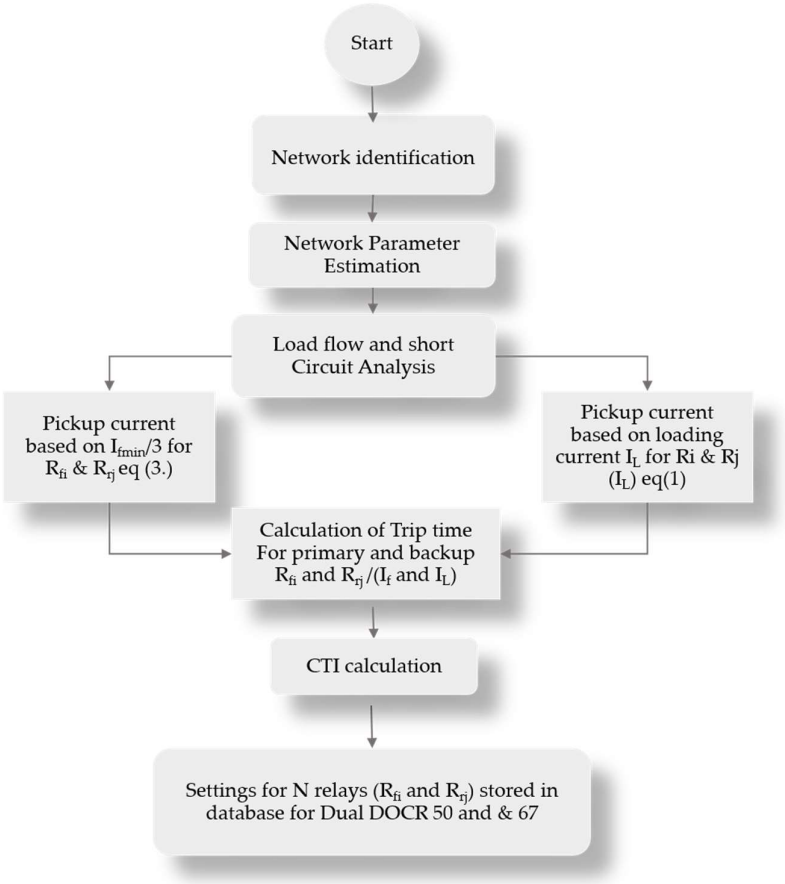


Figure 4: Offline Settings for *N*-bus Microgrid DOCR.

Once the network parameters are determined, the next step involves load flow and short circuit analysis. Generally, computer programs are used for load flow (LF) and short circuit (SC) analysis, that model the microgrid system in terms of equivalent impedances, slack bus, voltage-controlled bus, load bus, and equivalent sequence circuits. PF calculates respective bus voltages, branch currents, and line losses. Various standard power flow algorithms, e.g. Newton-Raphson (NR), Gauss-Seidel (GS), etc. [19], and extended power flow algorithms [20] can be used for LF, however, for the simplicity of analysis, we have employed the built-in power flow models available in DigSilent Powerfactory. Similarly, for short circuit analysis, symmetrical components and sequence circuit-based computer programs may be employed, however, within the scope of this work, we have used the built-in power factory NR method for the short circuit studies model [21].

Once line loadings and fault current computations are available the dual-stage settings for IDMT and DTOC elements are performed as described in section 2.1. The procedure is repeated for all relays in the microgrid model for potential possible configurations, and are stored in the memory of ICPU as shown in figure 4.

During the operation of the microgrid, the ICPU keeps on monitoring the network status as well as the status of DG availability (based on the circuit breaker status), DG protection itself is quite an extensive topic [22] and is not covered in the scope of this paper, hence we have assumed that the internal protection of DG is well in place and operational. Any fault in the DG will disconnect it for the microgrid network and ICPU will be able to detect this through the status of the circuit breaker. Similarly, ICPU can also distinguish between grid-connected and islanded modes of operation based on the circuit breaker installed at the point of common coupling (PCC). There exist many advanced methods for islanding detection [23], however, to keep the focus of the work well defined with the scope of DOCR protection, we have assumed that the islanding detection algorithm is well in place and operational, therefore, ICPU can detect islanding based on the status of the circuit breaker

Preprints (www.preprints.org) | NOT PEER-REVIEWED | Posted: 11 February 2021 doi:10.20944/preprints202102.0288.v1



available at the PCC. Referring to Figure 5, during the operation, the network changes will be detected by ICPU, and accordingly offline settings will be adopted for the incident conditions. The procedure keeps on repeating throughout the operation of the microgrid and the algorithm in figure 5 allows adapting the settings of the DOCR according to the incident conditions. It should be mentioned that in case if no change is detected the algorithm retains its previous settings, and therefore relay adapts new setting only if there are any significant changes in the network, i.e. transition from grid-connected mode to islanded mode or due to the addition/ loss of DG unit.

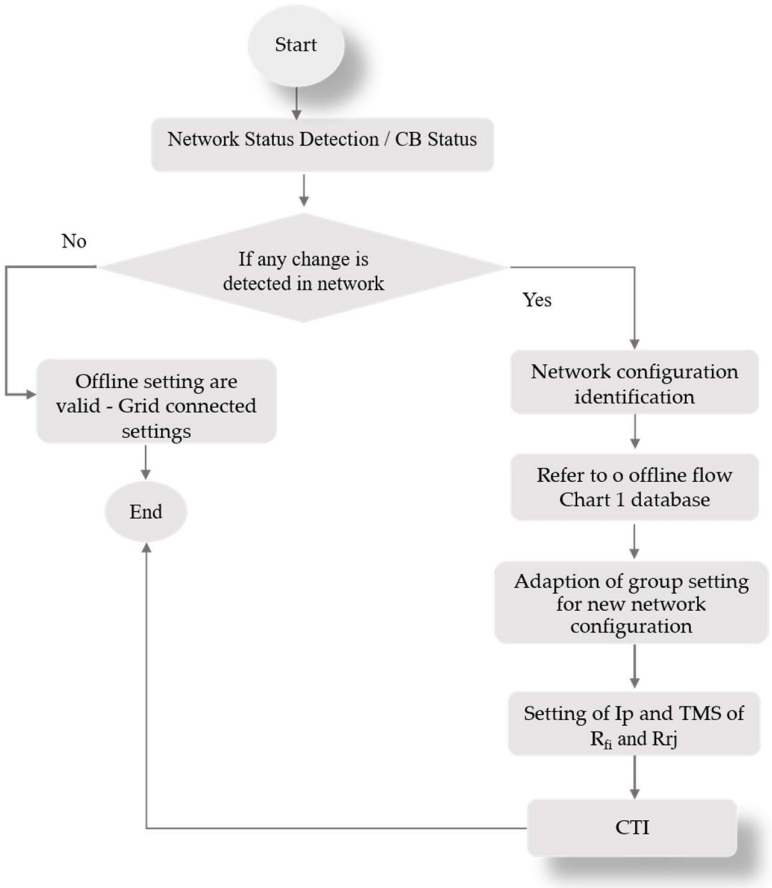


Figure 5: Adaptive algorithm for the overcurrent protection of *N*-bus Microgrid.

## 3. Test Model Parameters and Case Studies

### *3.1. Simulation Model Parameters and Case studies*

In order to validate the proposed methodology, the protection scheme presented above is implemented on the modified IEEE- 9 bus model [24, 25] and simulated in DigSilent Power Factory 2020. The model consists of four DGs, 9 buses, eight general types of load, and is connected with the utility grid at PCC as shown in figure 6 (a). Detailed specifications of the network parameters considered for the simulation are presented in Table 1. Three sample configurations of the test model in operation scenarios are shown in figures 6 (a) to (c). Figure 6 (a) shows the model in the grid-connected mode of operation whereas all four DGs are connected. In figure 6 (b), two arbitrary DGs (DG 2 and DG 4 are offline (out of service ). While in figure 6 (c), the network is operating in islanded mode, whereas all four DGs are connected in the system and the utility grid is offline. For these three sample cases, the LF and SC analysis are performed as described in section 2.2 and figure 5. The detailed values of LF and SC analysis are tabulated in Appendix 1.

Preprints (www.preprints.org) | NOT PEER-REVIEWED | Posted: 11 February 2021 doi:10.20944/preprints202102.0288.v1



Table 1: Model and simulation parameters

| Model Parameters | Values |
|---|---|
| Utility Grid | Maximum and minimum short circuit powers (300 MVA and 250 MVA) |
| DGs (1 to 4)<br>Type- 4 wind turbine | (2.77 MW 0.9 PF)<br>Maximum and minimum short circuit powers (5.5 MVA and 2.5 MVA) |
| Transformers ($T_1$ to $T_5$) | $T_1$ (47 MVA, 33 kV/ 11 kV),<br>$T_2$, $T_3$, $T_5$, $T_6$ ( 2.8 MVA 11 kV / 0.4 kV) |
| Loads ($L_1$ to $L_8$) | (1 MW, 0.1 MVar) |
| Lines (line 1 to Line 8 ) | 0.1529+*j*0.1406 Ω/km, each line is 0.5 km long |

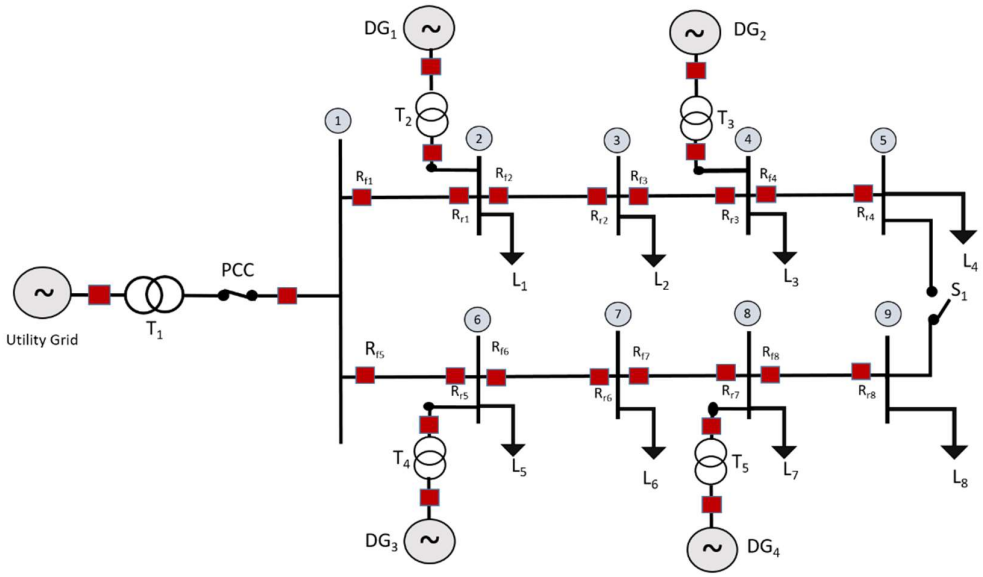


Figure 6 (a): Microgrid Test Model Modified- IEEE -9 bus system (case study 1)

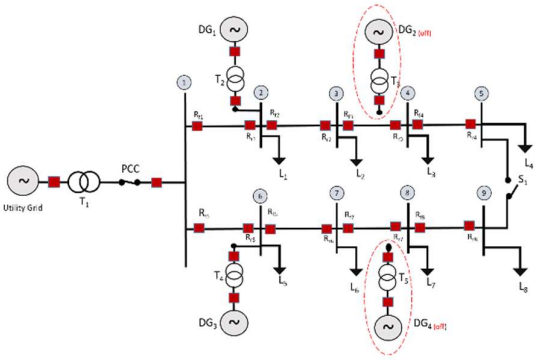

Figure 6 (b): Two DGs offline (Case study 2)

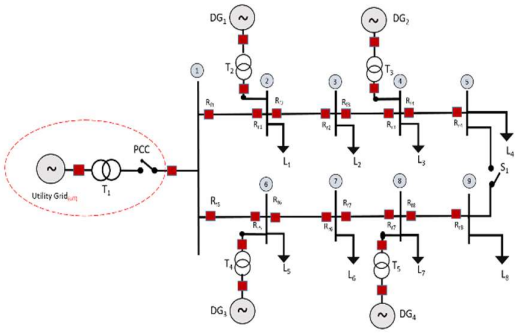

Figure 6 (c): Islanded mode (case study 3)

### *3.2. Relay Fault Current Analysis and offline settings:*

The above case studies are shown in Fig: 6 (a), (b), (c) are simulated for a 3 phase bolted fault condition of 0,1 Ω in each bus as well as in the middle of each line. Short circuit analysis is performed in Power Factory DigSilent software. For each case study the maximum and minimum short circuit current,

 doi:10.20944/preprints202102.0288.v1



voltage, and power values are recorded. With the help of short circuit data, the fault current seen by each forward and reverse relay for line 1 to line 4 for all three cases (case 1, case 2, and case 3) are given in Tables 2 to 4 respectively.

Table 2: Case 1 (Grid-Connected); Fault current at each forward and reverse relay for line 1 to line 4

| F4 | Fault Current (A) | F3 | Fault Current (A) | F2 | Fault Current (A) | F1 | Fault Current (A) |
|---|---|---|---|---|---|---|---|
| $R_{f1}$ | 5689 | $R_{f1}$ | 6243 | $R_{f1}$ | 6883 | $R_{f1}$ | 7623 |
| $R_{r1}$ | 5689 | $R_{r1}$ | 6243 | $R_{r1}$ | 6883 | $R_{r1}$ | 503 |
| $R_{f2}$ | 5901 | $R_{f2}$ | 6471 | $R_{f2}$ | 7131 | $R_{f2}$ | 243 |
| $R_{r2}$ | 5901 | $Rr_2$ | 6471 | $R_{r2}$ | 244 | $Rr_2$ | 243 |
| $R_{f3}$ | 5890 | $R_{f3}$ | 6464 | $R_{f3}$ | 250 | $R_{f3}$ | 250 |
| $R_{r3}$ | 5890 | $R_{r3}$ | 0,251 | $R_{r3}$ | 250 | $R_{r3}$ | 250 |
| $R_{f4}$ | 6134 | $R_{f4}$ | 0,006 | $R_{f4}$ | 0,006 | $R_{f4}$ | 0,007 |
| $R_{r4}$ | 0,005 | $R_{r4}$ | 0,006 | $R_{r4}$ | 0,006 | $R_{r4}$ | 0,007 |

Table 3: Case 2 (Grid-Connected with two DGs); Fault current at each forward and reverse relay for line 1 to line 4

| F4 | Fault Current (A) | F3 | Fault Current (A) | F2 | Fault Current (A) | F1 | Fault Current (A) |
|---|---|---|---|---|---|---|---|
| $R_{f1}$ | 5556 | $R_{f1}$ | 6083 | $R_{f1}$ | 6701 | $R_{f1}$ | 7407 |
| $R_{r1}$ | 5526 | $R_{r1}$ | 6083 | $R_{r1}$ | 6701 | $R_{r1}$ | 0,267 |
| $R_{f2}$ | 5819 | $R_{f2}$ | 6352 | $R_{f2}$ | 6977 | $R_{f2}$ | 0,019 |
| $Rr_2$ | 5819 | $R_{r2}$ | 6352 | $R_{r2}$ | 0,017 | $R_{r2}$ | 0,019 |
| $R_{f3}$ | 5808 | $R_{f3}$ | 6345 | $R_{f3}$ | 0,012 | $R_{f3}$ | 0,013 |
| $R_{r3}$ | 5808 | $R_{r3}$ | 0,011 | $R_{r3}$ | 0,012 | $R_{r3}$ | 0,013 |
| $R_{f4}$ | 5801 | $R_{f4}$ | 0,005 | $R_{f4}$ | 0,006 | $R_{f4}$ | 0,006 |
| $R_{r4}$ | 0,005 | $R_{r4}$ | 0,005 | $R_{r4}$ | 0,006 | $R_{r4}$ | 0,006 |

Table 4: Case 3 (Islanded Mode); Fault current at each forward and reverse relay for line 1 to line 4

| F4 | Fault Current (A) | F3 | Fault Current (A) | F2 | Fault Current (A) | F1 | Fault Current (A) |
|---|---|---|---|---|---|---|---|
| $R_{f1}$ | 496 | $R_{f1}$ | 502 | $R_{f1}$ | 507 | $R_{f1}$ | 512 |
| $R_{r1}$ | 496 | $R_{r1}$ | 502 | $R_{r1}$ | 767 | $R_{r1}$ | 514 |
| $R_{f2}$ | 751 | $R_{f2}$ | 759 | $R_{f2}$ | 256 | $R_{f2}$ | 254 |

Preprints (www.preprints.org) | NOT PEER-REVIEWED | Posted: 11 February 2021 doi:10.20944/preprints202102.0288.v1



| | | | | | | | |
|---|---|---|---|---|---|---|---|
| $Rr_2$ | 751 | $Rr_2$ | 759 | $Rr_2$ | 257 | $Rr_2$ | 254 |
| $R_{f3}$ | 749 | $R_{f3}$ | 758 | $R_{f3}$ | 257 | $R_{f3}$ | 255 |
| $R_{r3}$ | 749 | $R_{r3}$ | 275 | $R_{r3}$ | 275 | $R_{r3}$ | 255 |
| $R_{f4}$ | 1007 | $R_{f4}$ | 0,001 | $R_{f4}$ | 0,001 | $R_{f4}$ | 0,001 |

This information is critical to determine as the decision taken by each relay depends upon the value of the fault current it observes. Though there are 8 lines and 2 feeders in the model as shown in figure 6, however, due to similarity in structure and to make the analysis simpler, the load and DG power in both feeders are kept similar. Therefore, for the purpose of presentation, fault levels are shown only for feeder 1 relays from line1 to line 4. For instance, in each table (Tables 2 - 4), F1, F2, F3, etc. corresponds to the fault in the corresponding line such that F1 denotes the fault in line 1 as shown in figures 6 (a) to 6 (c). Similarly, $R_{f1}$ corresponds to the fault level seen by the forward relay at bus 1, and $R_{r1}$ corresponds to the fault level seen by the reverse relay at bus 1.

Figures 7 (a) to 7 (c) present the pictorial representation of fault current seen by each relay for faults at F1 to F4 as shown in figure 6. It may be emphasized that in the case of the conventional radial power system, fault levels of the subsequent relays follow the decreasing sequence, as we move from the source end to the load end. Therefore, it is very simple to configure the coordination of these relays, when DGs are not connected. However, in the case of microgrids, relays do not follow the sequence of increasing or decreasing currents at the subsequent neighboring relays, as DGs can also contribute to the fault current. For instance, it can be seen in figure 7 (a), for case 1, i.e. in the grid-connected scenario, the fault current seen by the forward relay $R_{f3}$ (green colored bar) is lowest in the start, increases in line 3, and then again decreases. This is due to the current contribution by DG2. Therefore, it is essential to configure these relays based on their respective LF and SC data, and thereby adjust their TMS to ensure the standard CTI, as defined by the adaptive algorithm presented in figure 5. A similar random trend of current contribution by DGs and associated relays in subsequent lines can also be observed in other cases, i.e. for case 2 (grid-connected with two DGs) and case 3 islanded mode of microgrid operation.

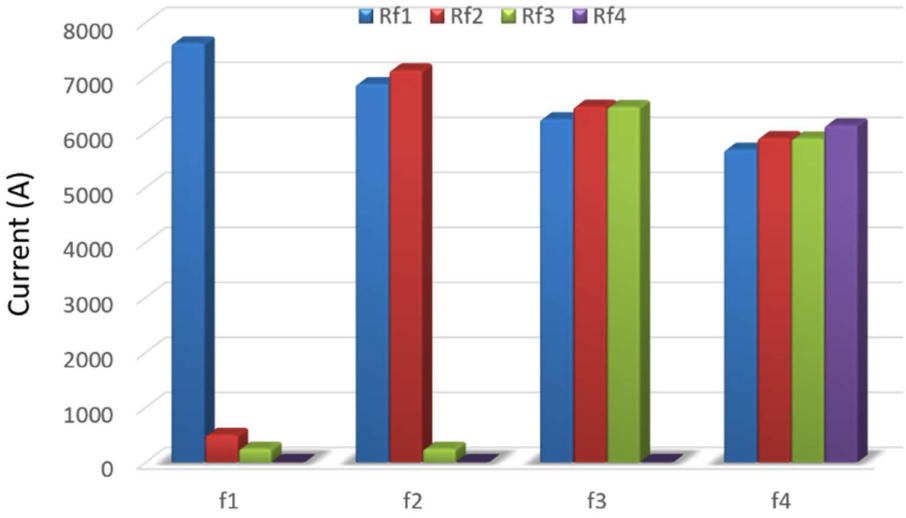

Preprints (www.preprints.org) | NOT PEER-REVIEWED | Posted: 11 February 2021 doi:10.20944/preprints202102.0288.v1



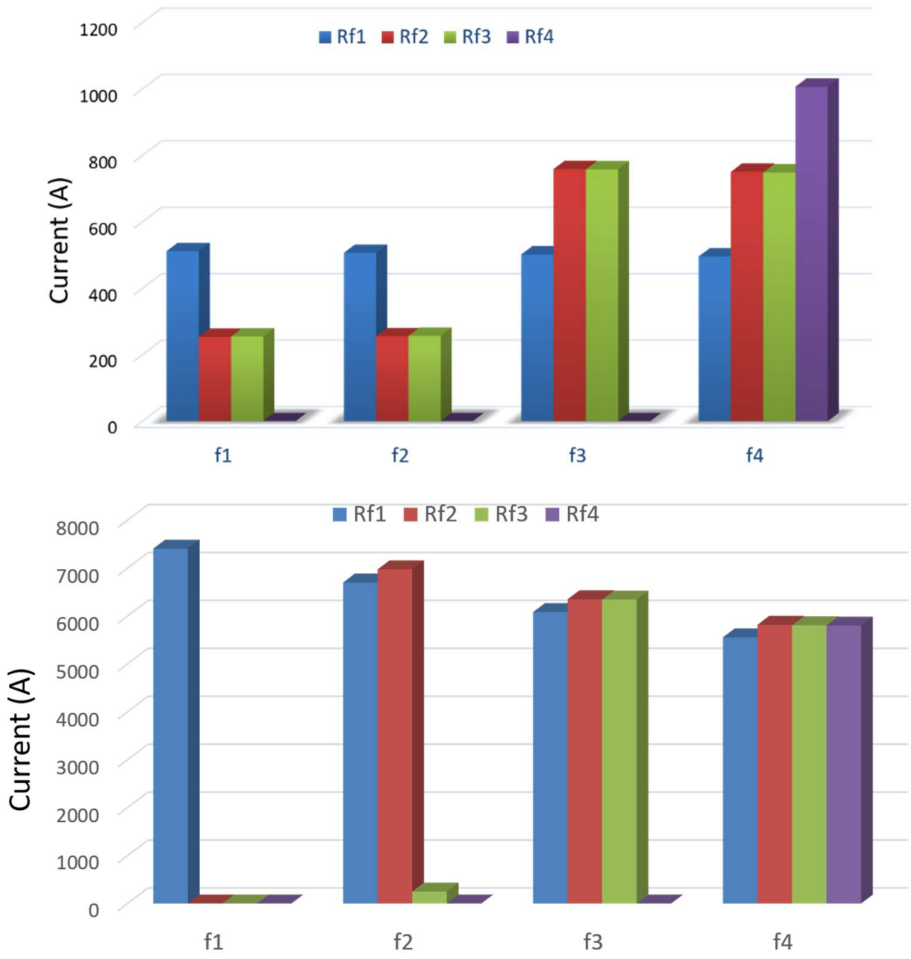


Figure 7. (a): Fault current seen by each forward relay during faults at different lines for Case 1: (Grid-connected mode of operation); (b): Fault current seen by each forward relay during faults at different lines for Case 2: (Grid-connected with two DGs); (c): Fault current seen by each forward relay during faults at different lines for Case 3: (Islanded mode of operation)

Moreover, from figures 7 (a) to 7 (c), it can be observed that the current levels seen by each relay for case 3 are significantly lower as compared to case 1 and case 2. This is because the main source of short circuit power, i.e. grid is not available and the microgrid is operating in the islanded mode of operation. Likewise, the fault currents and relay currents are analyzed for the second feeder from lines 5 to 8 for the corresponding forward and reverse relays. These faults current and relay currents are utilized to determine the pickup current and TMS settings as explained in design section 2. The designed values of dual-stage (IDMT and DTOC characteristics) for the presented case studies are shown in tables in Tables 5 to 7. It is also highlighted that the table presents the data for active relays only in a given configuration, for instance in all these tables, stage-2 (DTOC characteristics) are inactive. Similarly, for case 3 in Table 7 (islanded mode of operation), stage-2 is not required due to low currents, as the main source of high short circuit power, i.e. grid is unavailable.

Preprints (www.preprints.org) | NOT PEER-REVIEWED | Posted: 11 February 2021 doi:10.20944/preprints202102.0288.v1



Table 5: Pickup current and TMS for dual-stage DOCR for Case 1: (Grid-connected)

| DTOC Relay (Stage-2) | Pickup Current $Ipu^2$ (A) | TMS² | IDMT Relay (Stage-1) | Pickup Current $Ipu^2$ (A) | TMS² (s) |
|---|---|---|---|---|---|
| $R_f$ | 2420 | 0.35 | $R_{f1}$ | 440 | 0.42 |
| | | | $R_{r1}$ | 167 | 0.05 |
| $R_{f2}$ | 2270 | 0.25 | $R_{f2}$ | 320 | 0.32 |
| | | | $Rr_2$ | 81 | 0.11 |
| $R_{f3}$ | 2060 | 0.15 | $R_{f3}$ | 210 | 0. 20 |
| | | | $R_{r3}$ | 83 | 0.15 |
| $R_{f4}$ | 1950 | 0.05 | $R_{f4}$ | 110 | 0.05 |

Table 6: Pickup current and TMS for dual-stage DOCR for Case 2: (Grid-connected with two DGs)

| DTOC Relay (Stage-2) | Pickup Current $Ipu^2$ (A) | TMS² | IDMT Relay (Stage-1) | Pickup Current $Ipu^2$ (A) | TMS² (s) |
|---|---|---|---|---|---|
| $R_{f1}$ | 2360 | 0.35 | $R_{f1}$ | 210 | 0.5 |
| | | | $R_{r1}$ | 80 | 0.05 |
| $R_{f2}$ | 2190 | 0.25 | $R_{f2}$ | 320 | 0.32 |
| $R_{f3}$ | 2010 | 0.15 | $R_{f3}$ | 210 | 0. 20 |
| $R_{f4}$ | 180 | 0.05 | $R_{f4}$ | 110 | 0.05 |

Table 7: Pickup current and TMS for IDMT relays for Case 3: (Islanded Mode)

| IDMT Relay (Stage-2) | Pickup Current $Ipu^2$ (A) | TMS² (s) |
|---|---|---|
| $R_{f1}$ | 170 | 0.19 |
| $R_{r1}$ | 171 | 0.05 |
| $R_{f2}$ | 260 | 0.15 |
| $Rr_2$ | 85 | 0.09 |
| $R_{f3}$ | 250 | 0. 09 |
| $R_{r3}$ | 86 | 0.14 |
| $R_{f4}$ | 110 | 0.05 |

## 4. Results and Discussions

In the previous section, the offline calculations and dual-stage settings for DOCR for the overcurrent protection of IEEE 9-bus microgrid model have been computed. These settings have been stored in ICPU, and the offline algorithm (Fig. 5) adapts the respective settings based on the network configuration and incident scenario. Consequently, various scenarios have been evaluated after the application of the fault. Since the three-phase bolted fault is the most severe in the AC power system, therefore, the comparative simulations have been performed under the application of three-phase faults. The result section starts with the demonstration of the utility of two-stage settings over static single-stage settings. As discussed in the design section, two-stage settings allow us to achieve a lower tripping time, while maintaining the coordination among the neighboring relays.

Figure 8 (a) shows the characteristics curve for the setting of IEC inverse relay (IDMT) for grid connected-mode of operation when a fault is applied at line 4, i.e. $F_4$ (shown in figure 5). Similarly, figure 8 (b) shows the characteristic curve and tripping of the dual-stage setting with IDMT along with the DTOC characteristics. From Figures 8 (a) and 8 (b), it may be observed that during this fault, the forward relay $R_{f4}$, sees a current of 6.134 kA. This will generate the tripping signal and the overall relay operation time for clearing the $F_4$ fault is 0.09s for both single-stage and dual-stage relays. However, if for some reason $R_{f4}$ does not operate, $R_{f3}$ will wait for CTI and will come into action to

Preprints (www.preprints.org) | NOT PEER-REVIEWED | Posted: 11 February 2021 doi:10.20944/preprints202102.0288.v1



clear the fault. This trip time is significantly lower for the two-stage relay, i.e. 0.180s (figure 8 (b)), as compared to the single-stage IDMT relay, for which trip time is 0.406s (figure 8 (a)). This lower trip time has been achieved using relatively smaller CTI for the DTOC characteristics, i.e. 100ms. Therefore, two-stage characteristics allow us to achieve lower tripping time, consequently, the fault will stay in the microgrid system for a lower time, and associated hazards will be relatively lower.

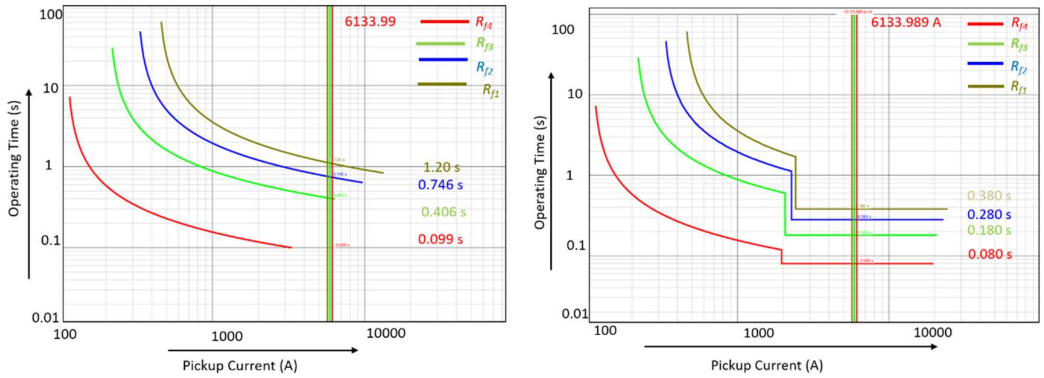


Figure 8: Characteristics curves for fault at line 4 for case 1 (grid- connected), (a): one-stage IDMT relay and (b): two-stage DOCR

These coordination settings have been further illustrated through figures 9 and 10. In these figures, forward relay $R_{f4}$ is kept out of service, and fault current characteristics seen by the forward relay $R_{f3}$ are plotted for both single-stage and dual-stage settings. Moreover, for the detailed comparison, electromagnetic (EMT) simulations are also shown. Figure 9. shows the relay characteristics and EMT simulation for single stage relay, while figure 10 shows the relay characteristics and EMT simulation for dual-stage stage relay. From the comparison of figures 9 and 10, it may be confirmed that for both EMT and RMS simulations (relay characteristics curve), dual-stage has lower tripping time, therefore exhibits superior performance in comparison to single stage relay.

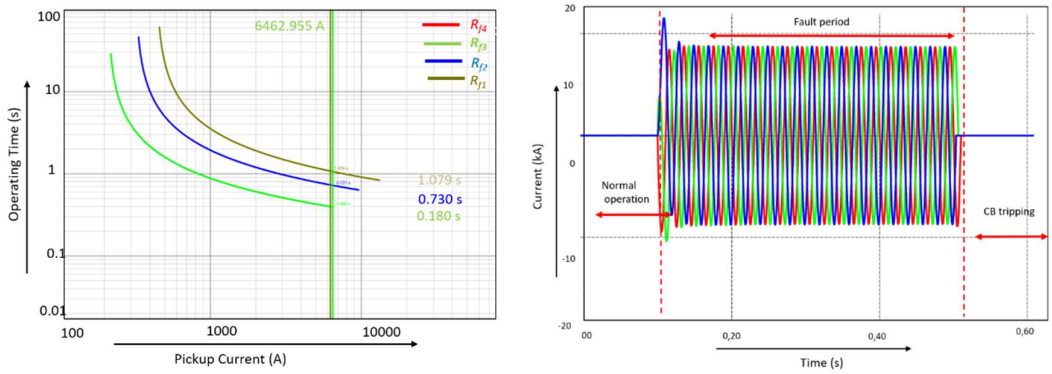


Figure 9: Fault at line 4, coordinated by the single-stage forward relay $R_{F3}$ for case 1 (grid-connected), (a): characteristic curve, (b): EMT simulation

Preprints (www.preprints.org) | NOT PEER-REVIEWED | Posted: 11 February 2021 doi:10.20944/preprints202102.0288.v1



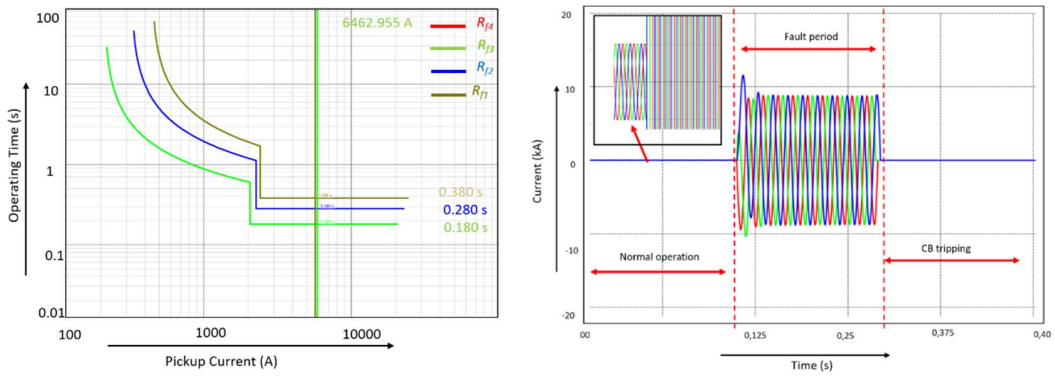


Figure 10: Fault at line 4, coordinated by the dual-stage forward relay $R_{F3}$ for case 1 (grid-connected) (a) characteristic curve, (b) EMT simulation

In the next scenario, grid-connected configuration with two DGs disconnected (case 2), static protection settings are compared with the proposed adaptive settings for fault $F_3$ in figures 11 (a) and 11 (b) respectively. Static settings imply that, though the relays are dual-stage, they are unable to update their settings with respect to the mode of operation, i.e. they do not encounter the effect of DG disconnection and these relays are still operating with the dual-stage grid-connected settings of the case 1. Alternatively, the proposed adaptive algorithm encompasses the effect of DG disconnection and updates the settings of the relays as discussed in section 2.

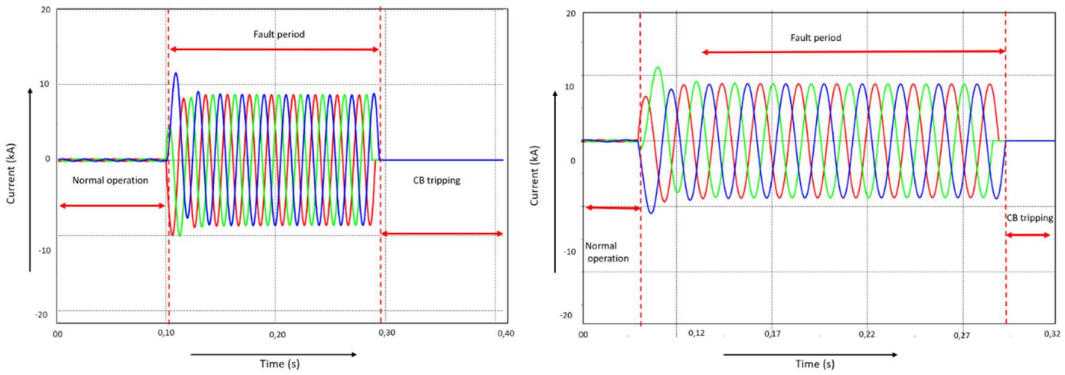


Figure 11: Fault at line 3, coordinated by the dual-stage forward relay $R_{F3}$ for case 2 (two DGs disconnected) (a) static dual-stage settings, (b) adaptive dual-stage settings

From the analysis of both settings in figure 11, it may be observed that the disconnection of two DGs does not affect the settings significantly. Consequently, the trip time achieved through the proposed method is somewhat similar to the static scheme. This is because DGs have a very small short circuit capacity in comparison to the grid, therefore, overall tripping time does not change significantly in this scenario.

However, an absence of the grid in the case of the islanded mode of operation (case 3) will drastically change the scenario. Figure 12 shows the comparison between static settings and the proposed adaptive settings in the islanded mode of operation for a fault at bus 3. Again, static settings do not take into account the network dynamics, therefore, dual-stage relays are still configured with the same old setting as for case 1, and case 2. Alternatively, the adaptive settings update the pickup currents and TDS of relays following the proposed algorithm as shown in figure 5 and Table 7.

From the comparison of figure 12 (a) and 12 (b), it may be observed that for the same level of fault, forward relay $R_{F3}$ clears fault much earlier in the proposed adaptive settings (Fig. 12 (b)) compared to the static settings shown in Figure 12 (a). Therefore, it may be concluded that the proposed algorithm allows achieving better protection performance in accordance with the dynamically changing network conditions.

Preprints (www.preprints.org) | NOT PEER-REVIEWED | Posted: 11 February 2021 doi:10.20944/preprints202102.0288.v1



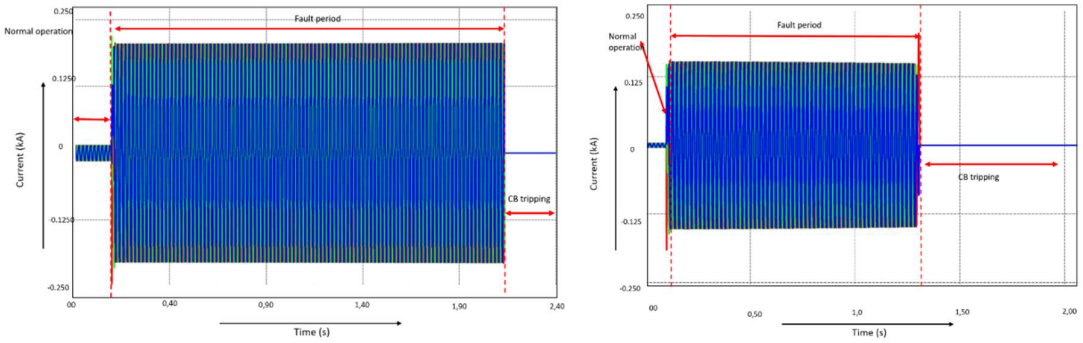


Figure 12: Fault at line 3, coordinated by the dual-stage forward relay $R_{F3}$ for case 3 (islanded mode of operation) (a) static dual-stage settings, (b) adaptive dual-stage settings

## 5. Conclusion

An adaptive scheme for the overcurrent protection of AC microgrids using dual-stage DOCR is presented in this work. It has been demonstrated that the proposed scheme has the capability to dynamically configure the settings of its relays based on the changing network conditions. The operation of the scheme is demonstrated in grid-connected, islanded and variable distributed generation scenarios have been demonstrated. The up-gradation of DOCR settings in the proposed scheme allows us to reduce the tripping times of the relays, thereby reduce the associated high-current hazards in the system. Moreover, the proposed scheme also maintains the desired coordination for backup relaying applications. The proposed scheme may be further extended to online/ hybrid offline-online adaption, using programmable numeric relays hardware-in-loop HIL platforms.

**Acknowledgments:** This work was funded by a "Villum Investigator grant" (no. 25920) from The Villum Fonden Denmark and Balochistan University of Engineering and Technology Khuzdar, Pakistan.

**Conflicts of Interest:** The authors and work do not have a conflict of interest.

## Appendix A

**Table A1: Short Circuit Analysis for case study 1: Grid Connected operation of AC Microgrids**

| Case 3 (Islanded with all DGs) | Max. Short Circuit Current (kA) | Min. Short Circuit Current (kA) | Voltage at bus(during max short circuit ) (kV) | Voltage at bus (during min short circuit (kV) | Short circuit power max (MW) | Short circuit power min (MW) |
|---|---|---|---|---|---|---|
| Bus 1 | 8,532 | 8,19 | 1,48 | 1,42 | 162,60 | 156,10 |
| Bus 2 | 7,75 | 7,44 | 1,34 | 1,29 | 147,64 | 141,67 |
| Bus 3 | 7,03 | 6,73 | 1,22 | 1,17 | 133,98 | 128,23 |
| Bus 4 | 6,24 | 6,12 | 1,11 | 1,06 | 122,33 | 116,66 |
| Bus 5 | 5,86 | 5,57 | 1,02 | 0,96 | 111,68 | 106,08 |
| Bus 6 | 7,75 | 7,44 | 1,34 | 1,29 | 147,64 | 141,67 |
| Bus 7 | 7,55 | 7,20 | 1,31 | 1,25 | 143,83 | 137,09 |
| Bus 8 | 6,84 | 6,49 | 1,18 | 1,12 | 130,26 | 123,69 |
| Bus 9 | 6,20 | 5,86 | 1,07 | 1,02 | 118,13 | 111,71 |
| Line1 | 8,13 | 7,80 | 0,81 | 0,78 | 154,83 | 148,65 |
| Line2 | 7,38 | 6,66 | 0,74 | 0,71 | 140,53 | 134,69 |
| Line3 | 6,71 | 6,06 | 0,67 | 0,64 | 127,92 | 122,22 |
| Line4 | 6,13 | 5,54 | 0,61 | 0,58 | 116,79 | 111,15 |

Preprints (www.preprints.org) | NOT PEER-REVIEWED | Posted: 11 February 2021 doi:10.20944/preprints202102.0288.v1



| | | | | | | |
|---|---|---|---|---|---|---|
| Line5 | 8,13 | 7,80 | 0,81 | 0,78 | 154,83 | 148,65 |
| Line6 | 7,65 | 7,32 | 0,77 | 0,73 | 145,84 | 139,51 |
| Line7 | 7,18 | 6,83 | 0,72 | 0,68 | 136,74 | 130,09 |
| Line8 | 6,50 | 6,16 | 0,65 | 0,62 | 123,93 | 117,43 |

**Table A2: Short Circuit Analysis for case study 2: Grid-Connected Mode with two DGs**

| Case 3 (Islanded with all DGs) | Max. Short Circuit Current (kA) | Min. Short Circuit Current (kA) | Voltage at bus(during max short circuit ) (kV) | Voltage at bus (during min short circuit (kV) | Short circuit power max (MW) | Short circuit power min (MW) |
|---|---|---|---|---|---|---|
| Bus 1 | 8,05 | 7,70 | 1,39 | 1,33 | 153,29 | 146,79 |
| Bus 2 | 7,30 | 6,99 | 1,26 | 1,21 | 139,08 | 133,12 |
| Bus 3 | 6,62 | 6,32 | 1,15 | 1,09 | 126,10 | 120,39 |
| Bus 4 | 6,04 | 5,74 | 1,05 | 0,99 | 114,99 | 109,40 |
| Bus 5 | 5,53 | 5,24 | 0,96 | 0,91 | 105,44 | 99,93 |
| Bus 6 | 7,30 | 6,99 | 1,26 | 1,21 | 139,08 | 133,12 |
| Bus 7 | 7,12 | 6,77 | 1,23 | 1,17 | 135,59 | 128,96 |
| Bus 8 | 6,48 | 6,14 | 1,12 | 1,06 | 123,46 | 117,03 |
| Bus 9 | 5,90 | 5,58 | 1,02 | 0,97 | 112,49 | 106,22 |
| Line1 | 7,66 | 7,33 | 0,77 | 0,73 | 145,91 | 139,73 |
| Line2 | 6,74 | 6,64 | 0,69 | 0,66 | 132,33 | 126,52 |
| Line3 | 6,32 | 6,02 | 0,63 | 0,60 | 120,32 | 114,68 |
| Line4 | 5,64 | 5,48 | 0,58 | 0,55 | 110,03 | 104,48 |
| Line5 | 7,66 | 7,33 | 0,77 | 0,73 | 145,91 | 139,73 |
| Line6 | 7,21 | 6,88 | 0,72 | 0,69 | 137,42 | 131,15 |
| Line7 | 6,78 | 6,44 | 0,68 | 0,64 | 129,27 | 122,74 |
| Line8 | 6,18 | 5,85 | 0,62 | 0,58 | 117,75 | 111,40 |

**Table A3- Short Circuit Analysis for case study 3: Islanded Mode Operation of AC Microgrids**

| Case 3 (Islanded with all DGs) | Max. Short Circuit Current (kA) | Min. Short Circuit Current (kA) | Voltage at bus(during max short circuit ) (kV) | Voltage at bus (during min short circuit (kV) | Short circuit power max (MW) | Short circuit power min (MW) |
|---|---|---|---|---|---|---|
| Bus 1 | 1,02 | 1,02 | 0,18 | 0,18 | 19,52 | 19,51 |
| Bus 2 | 1,02 | 1,02 | 0,18 | 0,18 | 19,52 | 19,51 |
| Bus 3 | 1,02 | 1,02 | 0,18 | 0,18 | 19,40 | 19,38 |
| Bus 4 | 1,01 | 1,01 | 0,18 | 0,17 | 19,27 | 19,25 |
| Bus 5 | 1 | 1 | 0,17 | 0,17 | 19,02 | 18,99 |
| Bus 6 | 1,02 | 1,02 | 0,18 | 0,18 | 19,52 | 19,51 |
| Bus 7 | 1,02 | 1 | 0,18 | 0,18 | 19,51 | 19,50 |
| Bus 8 | 1,02 | 1,02 | 0,18 | 0,18 | 19,38 | 19,36 |
| Bus 9 | 1 | 1 | 0,17 | 0,17 | 19,13 | 19,10 |
| Line1 | 1,02 | 1,02 | 0,10 | 0,10 | 19,52 | 19,51 |
| Line2 | 1,02 | 1,02 | 0,10 | 0,10 | 19,46 | 19,44 |
| Line3 | 1,01 | 1,01 | 0,10 | 0,10 | 19,33 | 19,31 |
| Line4 | 1 | 1 | 0,10 | 0,10 | 19,14 | 19,12 |
| Line5 | 1,02 | 1,02 | 0,10 | 0,10 | 19,52 | 19,51 |
| Line6 | 1,02 | 1,02 | 0,10 | 0,10 | 19,52 | 19,51 |
| Line7 | 1,02 | 1,02 | 0,10 | 0,10 | 19,45 | 19,43 |

| | | | | | | |
|---|---|---|---|---|---|---|
| Line8 | 1,01 | 1,01 | 0,10 | 0,10 | 19,25 | 19,23 |

## References


1. D. He and Y. Li, "Overview of worldwide wind power industry," in *Strategies of Sustainable Development in China's Wind Power Industry*, ed: Springer, 2020, pp. 29-60.
2. P. Balakrishnan, M. S. Shabbir, A. F. Siddiqi, and X. Wang, "Current status and future prospects of renewable energy: A case study," *Energy Sources, Part A: Recovery, Utilization, and Environmental Effects,* vol. 42, pp. 2698-2703, 2020.
3. IEA. Renewables 2020 [Online]. Available: https://www.iea.org/reports/renewables-2020
4. Z. Li and M. Shahidehpour, "Role of microgrids in enhancing power system resilience," in *2017 IEEE Power & Energy Society General Meeting*, 2017, pp. 1-5.
5. A. Hirsch, Y. Parag, and J. Guerrero, "Microgrids: A review of technologies, key drivers, and outstanding issues," *Renewable and sustainable Energy reviews,* vol. 90, pp. 402-411, 2018.
6. M. Nasir and A. A. Bhatti, "A micro computer-based methodology for distance protection on long UHV transmission lines using symmetrical components," in *2012 Asia-Pacific Power and Energy Engineering Conference*, 2012, pp. 1-6.
7. N. Hussain, M. Nasir, J. C. Vasquez, and J. M. Guerrero, "Recent developments and challenges on AC microgrids fault detection and protection systems–a review," *Energies,* vol. 13, p. 2149, 2020.
8. P. Mahat, Z. Chen, B. Bak-Jensen, and C. L. Bak, "A simple adaptive overcurrent protection of distribution systems with distributed generation," *IEEE Transactions on Smart Grid,* vol. 2, pp. 428-437, 2011.
9. F. Coffele, C. Booth, and A. Dyśko, "An adaptive overcurrent protection scheme for distribution networks," *IEEE Transactions on Power Delivery,* vol. 30, pp. 561-568, 2014.
10. A. A. Memon and K. Kauhaniemi, "An Adaptive Protection for Radial AC Microgrid Using IEC 61850 Communication Standard: Algorithm Proposal Using Offline Simulations," *Energies,* vol. 13, p. 5316, 2020.
11. D. S. Kumar, D. Srinivasan, A. Sharma, and T. Reindl, "Adaptive directional overcurrent relaying scheme for meshed distribution networks," *IET Generation, Transmission & Distribution,* vol. 12, pp. 3212-3220, 2018.
12. H. Lin, K. Sun, Z.-H. Tan, C. Liu, J. M. Guerrero, and J. C. Vasquez, "Adaptive protection combined with machine learning for microgrids," *IET Generation, Transmission & Distribution,* vol. 13, pp. 770-779, 2019.
13. H. Lin, J. M. Guerrero, C. Jia, Z.-h. Tan, J. C. Vasquez, and C. Liu, "Adaptive overcurrent protection for microgrids in extensive distribution systems," in *IECON 2016-42nd Annual Conference of the IEEE Industrial Electronics Society*, 2016, pp. 4042-4047.
14. A. I. Atteya, A. M. El Zonkoly, and H. A. Ashour, "Adaptive protection scheme for optimally coordinated relay setting using modified PSO algorithm," *Journal of Power Technologies,* vol. 97, pp. 463-469, 2017.
15. J.-C. Gu, H.-Y. Chun, Y. Yen, and M.-T. Yang, "Apply setting group function of IED in protection management systems for microgrid reconfiguration," in *2019 International Youth Conference on Radio Electronics, Electrical and Power Engineering (REEPE)*, 2019, pp. 1-6.
16. W. Zhao, O. Alexandre, S. Bin, and C. Yao, "Research on close-loop simulation for centralized coordination of protection settings," in *2012 China International Conference on Electricity Distribution*, 2012, pp. 1-6.
17. S. IEC, "Measuring relays and protection equipment Part 1: Common requirements," *IEC 60255-1,* 2009.
18. I. I. A. S. Industrial and C. P. S. Committee, *IEEE Recommended Practice for Protection and Coordination of Industrial and Commercial Power Systems: Approved September 19, 1985, Reaffirmed June 27, 1991 IEEE Standards Board: Approved February 28, 1986, Reaffirmed December 9, 1991, American National Standards Institute*: Ieee, 1986.
19. H. Saadat, *Power system analysis* vol. 2: McGraw-hill, 1999.
20. G. D. A. Tinajero, M. Nasir, J. C. Vasquez, and J. M. Guerrero, "Comprehensive power flow modelling of hierarchically controlled AC/DC hybrid islanded microgrids," *International Journal of Electrical Power & Energy Systems,* vol. 127, p. 106629, 2021.
21. F. M. Gonzalez-Longatt and J. L. Rueda, *PowerFactory applications for power system analysis*: Springer, 2014.

22. U. Shahzad, S. Kahrobaee, and S. Asgarpoor, "Protection of distributed generation: challenges and solutions," *Energy and Power Engineering,* vol. 9, p. 614, 2017.
23. M.-S. Kim, R. Haider, G.-J. Cho, C.-H. Kim, C.-Y. Won, and J.-S. Chai, "Comprehensive review of islanding detection methods for distributed generation systems," *Energies,* vol. 12, p. 837, 2019.
24. A. Sharma and B. K. Panigrahi, "Phase fault protection scheme for reliable operation of microgrids," *IEEE Transactions on Industry Applications,* vol. 54, pp. 2646-2655, 2017.
25. W. K. Najy, H. H. Zeineldin, and W. L. Woon, "Optimal protection coordination for microgrids with grid-connected and islanded capability," *IEEE Transactions on industrial electronics,* vol. 60, pp. 1668-1677, 2012.